Morphological details contribute to neuronal response variability within the same cell type

Kevin Sandbote[1], Ihor Arkhypchuk[1], Jutta Kretzberg[1,2,3*],

1 Computational Neuroscience, Department of Neuroscience, Faculty VI, University of Oldenburg, Oldenburg, Germany
2 Cluster of Excellence Hearing4all, Department of Neuroscience, Faculty VI, University of Oldenburg, Oldenburg, Germany
3 Research Center Neurosensory Science, Carl von Ossietzky Universität Oldenburg, Oldenburg, Germany

* jutta.kretzberg@uni-oldenburg.de

Abstract

A large body of literature offers an explanation on how biophysical diversity and variable branching patterns of neurons contribute to degeneracy, and therefore enable multiple solutions for a characteristic neuronal response. The specific influence of finer morphological details, such as diameter and length of dendritic branches, on response variability is yet unclear. In this study, we address this question using a model database approach with spatially extended, conductance-based compartmental models to study variability of response features, such as resting membrane potential, input resistance, spike count, first spike latency, spike height, and spike width. Using 15 reconstructed morphologies of leech touch cells with fixed branching patterns, we identified several thousands of parameter sets that reproduced the experimentally measured response features of all the tested morphologies. Even when the biophysical parameters were kept equal across reconstructed morphologies, variability in response features arose from the morphological details. Systematically varying the distribution of ion channels across the neuronal membrane revealed that all spike response features are influenced by the location of spike initiation zones with higher conductance density. Nevertheless, biologically plausible responses can arise from different locations of spike initiation zones and even homogeneous distribution of ion channels. Furthermore, comparing the simulated spike responses from two morphological subtypes of leech touch cells revealed that the previously published systematic differences cannot be explained by the morphological differences alone. A larger total conductance was required to reproduce the experimental finding of an increased spike count and a larger spike amplitude in a morphological subtype with a larger membrane area. In conclusion, biophysical properties, morphological details, and ion channel distribution across the membrane all interact in their contribution to the functionality and response variability of neurons of the same cell type.

Author summary

Neurons of the same type can exhibit differences in their shape or their biophysical properties. This variability, known as degeneracy, allows the nervous system to function reliably through many alternative mechanisms. While differences in ion channel

properties and coarse branching patterns are well-understood contributors to response variability, the influence of fine morphological details remains less clear. Using computational models of touch-sensitive neurons in the leech, we examined how neuronal shape, electrical properties, and the location of spike initiation zones affect their spiking activity. Based on 15 reconstructed neurons, we created thousands of models that reproduced experimentally observed activity. Even with identical electrical properties, we found that small morphological differences alone produced variability in spike timing, size, and number. Furthermore, realistic responses were obtained with different spike initiation sites and from uniformly distributed ion channels. Finally, to reproduce the systematic differences observed between two neuronal subtypes, our models required not only morphological differences but also distinct total membrane conductances. Our results reveal how morphology, ion channel distribution, and electrical properties interact to generate variability in neuronal responses, highlighting multiple pathways by which nervous systems achieve reliable function.

Introduction

The brain is often compared to a computer, suggesting that its components exhibit algorithmic functionality and deterministic behavior [1]. However, the idea that brains are built of many identical neurons is a fallacy, since cell-to-cell variability in neuronal responses is observed in nervous systems across species, e.g. in hippocampal neurons in rats [2], the visual system in drosophila [3], the stomatogastric nervous system of lobsters [4] and the nervous system of leeches [5–9]. In addition to this functional response variability, morphological variability in dendritic and axonal structure even within a defined cell type was reported by many studies [10–13]. The multiple sources of neuronal variability do not necessarily impair neuronal functionality, because functional network behavior can result from various combinations of neuronal configurations as was shown in experimental and modeling studies [14–16]. The concept of degeneracy, in which distinct structural configurations lead to similar functional outcomes, has emerged as a key principle exemplifying how biological systems maintain robust performance despite underlying variability [17]. In the context of neural circuits, degeneracy enables flexible computation and resilience to perturbations [18, 19].

Computational modeling has long been a cornerstone of neuroscience research. Modeling approaches, such as the Hodgkin-Huxley formalism [20, 21], often aimed to identify a single set of "optimal" parameters that reproduced a "typical" experimental observation. While powerful, such models do not always capture the broad range of observed biological variability. Increasingly, studies adopt a database modeling approach, in which large databases of conductance-based models were systematically examined to demonstrate that diverse combinations of ionic and synaptic properties can generate functionally similar network dynamics and neuronal outputs [14, 22–25]. These findings led to the understanding of degeneracy and variability, even within cells of the same type. While progress in characterizing the influence of biophysical and synaptic parameters has been substantial, the role of morphological details in shaping cell to cell response feature variability remains underexplored. Existing computational studies have focused primarily on variability between different cell types and variability in dendritic arborization patterns [11, 26–29], leaving a gap in the understanding of how variability within a fixed arborization pattern affects neuronal responses features of a specific cell type.

The leech nervous system provides a very accessible platform to investigate this question. It is traditionally considered stereotyped and consists of segmentally repeated ganglia with well-characterized and individually identifiable neurons [30]. The mechanosensory touch cell (T cell) encodes light tactile stimulation of the leech skin

with its spike count and first spike latency [31]. While the same individual T cell responds very precisely to repeated skin stimulation, the responses vary widely between neurons of this cell type [9, 32]. Early studies on leech mechanosensory neurons revealed, that T cells exhibit two distinct morphological subtypes, innervating different regions of the skin: T cells with one root process innervating the skin (1RP) and T cells with two root processes innervating the skin (2RP) [33]. More recent studies find that these morphological subtypes are contributing to the cell-to-cell variability with systematically different response features [13]. Meiser et al. speculated, that the systematically higher spike counts and larger spike amplitudes observed in 2RP cells are likely caused by a larger area of active membrane compared to 1RP cells [13]. This hypothesis cannot be tested experimentally because (to our knowledge) there are no established antibody staining methods for leech neurons capable of marking ion-channels or cell structures associated with spike initiation zones (SIZ), as was conducted previously in other species [34, 35]. Therefore, the distribution of voltage-dependent ion channels across the membrane of T cells can only be inferred indirectly from experimental and modeling studies. Previous studies suggested that a T cell has at least two SIZs, one (or more) in their distal processes innervating the skin and one (or more) SIZ proximal to its soma within the ganglion [36, 37]. Furthermore, a recently published single-compartment model of the T cell was able to reproduce typical response features, but systematically failed to reproduce the experimentally observed first spike latency, suggesting that spikes are not generated in the soma [38]. Hence, in this study we use a multi-compartmental modeling approach that incorporates spatial structure and ion channel distribution, to analyze their impact on spike generation and to explain systematic differences in response features between the two morphological subtypes.

In this study, we investigate how morphological details within a fixed branching pattern influence response variability in the leech T cell. Using a combination of reconstructed morphologies, electrophysiological recordings, and conductance-based modeling, we systematically assess how fine-scale morphological differences affect a cell's response to electrical stimulation. Furthermore, our study sheds light on systematic differences in the response patterns of T cell morphological subtypes. By systematically varying biophysical parameters and analyzing responses from a population of reconstructed morphologies, we isolate morphological variability from biophysical factors, and aim to clarify its specific contribution to functional variability.

Results

Leech T cells typically respond with short bursts of action potentials when their soma is electrically stimulated. However, the number, timing and shape of the action potentials vary between individual T cells. In order to investigate the influence of detailed morphological diversity on neuronal response variability, we generated and analyzed a large database of parameter sets that produced biologically plausible responses when applied to the reconstructed morphology of a leech T cell, rather than minimizing specific error values for the compartmental model. We defined a parameter set as *valid* and its model output as *biologically plausible*, if all analyzed response feature values were within the experimentally observed range based on 60 intracellular recordings of T cells [13]. The resting membrane potential and the input resistance were considered as subthreshold response features. The spike features were determined in response to a 500 ms long current injection of +1.5 nA into the soma. They comprised the spike count, the first spike latency, the spike height, and the repolarization duration, which we defined as the time between the peak of the second spike and the local minimum of the respective afterhyperpolarization (see Methods for details). All responses were measured in the soma of the cell, both in experimental data and in our simulations.

To test our hypothesis — that both biophysical and morphological properties contribute to neuronal response variability within the same cell type — required a multi-step approach. Firstly, we applied a large database of parameter sets to the same reconstructed morphology of a T cell to assess the contribution of variable biophysical properties. Secondly, three example parameter sets were applied to a population of 15 reconstructed T cell morphologies that differed in morphological details, such as diameters and length of cellular processes (S1 Fig and S2 Fig), to quantify the contribution of their morphological details to response feature variability. Since the spatial distribution of ion channels across the membrane of T cells is unknown, we compared different channel distribution configurations in the third step of the analysis to test whether our results depended critically on a specific location of the spike initiation zone. Finally, we investigated whether the experimentally observed systematic differences in response features between two subtypes (1RP and 2RP) of T cells could be explained by the morphological differences alone or if they require a difference in total membrane conductance.

Many parameter sets reproduce T cell responses

We began the parameter sweep with a multi-compartment model of a 1RP T cell, and placed the SIZ in the single process which innervates the leech's skin. Fig 1A shows the original microscopic image of this T cell, and Figure 1B displays the reconstructed morphology, in which all fine branches were removed and the anterior, posterior and root process were trimmed to ensure the same branching pattern and similar total length in all reconstructed morphologies (see Methods). We tested 48,828,125 parameter sets (all combinations of 11 parameters with 5 values each, Table 2) for this morphology and found that 1,859,170 sets yielded valid responses. Fig 1C shows an example of a biologically realistic response simulation obtained with the reconstructed morphology shown in Fig 1B. We then applied these valid sets to a population of 15 models based on individual reconstructed morphologies. This yielded 33,958 parameter sets that generated valid responses across all reconstructed morphologies (S1 Fig and S2 Fig) in the population.

Fig 1. T cell morphology and simulated response. A) Image of a 1RP T cell stained with neurobiotin. Magenta lines indicate the part of the morphology that was reconstructed. B) Morphological reconstruction of a leech T cell with one root process (1RP), in which the SIZ was located in the standard configuration. Diameters of compartments are not drawn to scale. See reconstruction 5 in S1 Fig for a figure version indicating diameters. The main branching pattern consisting of soma, main process, central process, anterior process, posterior process, an one root process, is the same for all 1RP morphologies (S1 Fig). C) Simulated response of this reconstructed T cell morphology measured in the soma. D) Stimulus protocol of the current injection (500 ms long pulses of -1.5 nA and 1.5 nA) into the soma, which was used in experiments and simulations throughout this study. E-F) Cell image, reconstruction and simulated response for a 2RP morphology. See reconstruction 5 in S2 Fig for a figure version indicating diameters. The main branching pattern of all 2RP morpholgies consist of the same processes as the 1 RP morphologies, plus an additional anterior root process (S2 Fig).

To isolate the contribution of biophysical diversity on response variability, we applied all parameter sets that yielded biologically plausible responses for the whole population, to the morphological reconstruction shown in Fig 1B. Different response features exhibited distinct degrees of variability (Fig 2). The variability of the resting membrane potential in the simulations obtained with this individual morphology

covered 30% of the range observed in the experiments with n=60 T cells (Fig 2A). The range of input resistance represented 17% of the range observed in the experiments (Fig 2B). Our model generated spike counts ranging from 2 to 9 spikes for all valid sets applied to this reconstructed morphology (Fig 2C). Although approximately 75% of the experimentally observed data were found in this range, some of the remaining experimental recordings yielded much higher spike counts, even up to 28 spikes in one cell. The simulated first spike latencies ranged from 6.2 ms to 9.2 ms for this reconstructed morphology, covering 13% of the variability observed in experiments (Fig 2D). The variability of spike height in the simulations represented 35% of the range from the smallest to the largest spikes in our datasets (Fig 2E). Simulated repolarization duration spanned from 3.9 ms to 6.1 ms, corresponding to 42% of the experimental range and covering rather the longer durations (Fig 2F).

Fig 2. Response variability caused by biophysical diversity applied to the same reconstructed morphology. Boxplots comparing response feature values of experimentally recorded n = 60 T cells (blue) to the model responses obtained for n = 33,958 parameter sets applied to the reconstructed morphology shown in Fig 1B (brown). The shown response features are A) resting membrane potential (3 outliers in model data), B) input resistance, C) spike count (in 500 ms, 2 outliers in experimental data, 281 outliers in model data), D) first spike latency (4 outliers in experimental data, 777 outliers in model data), E) spike height (448 outliers in model data), F) repolarization period (4 outliers in experimental data). In panel D, the y-axis was scaled for improved visibility, cutting off four outliers in latency from the experimentally obtained dataset (27.7 ms, 20.3 ms, 16.5 ms and 15.1 ms).

Our results show that a biologically plausible T cell response can arise from many different biophysical parameter sets. This supports the notion that T cells exhibit biophysical diversity, contributing to the observed cell-to-cell variability.

The variability in the simulated responses did not cover the entire experimentally observed range for any of the response features. This could be expected because the tested biophysical parameter space was limited to five different values for each conductance and reversal potential parameter, and no ion-channel kinetics were varied. Hence, varying additional biophysical parameters could introduce even higher response variability when applied to the same reconstructed morphology.

Morphological details contribute to response feature variability

Having examined variability due to multiple parameter sets applied to a single morphology, we next analyzed the variability caused by differences in morphological details. According to our criteria, 33,958 of the tested parameter sets generated plausible T cell responses for the entire population of 15 reconstructed morphologies. In this population, we included both morphological subtypes of T cells, eight 1RP and seven 2RP cells (See Fig 1 for one example of each morphological subtype, and S1 Fig and S2 Fig for the entire population). Applying the same parameter set to the population allowed us to isolate the impact of morphological details on response variability. Here, we illustrate this approach with three different parameter sets (Table 2 in Methods) which yielded systematically different spike counts, representing T cells with high, medium, and low activity, respectively (Fig 3).

The variability observed in the RMP was only ∼1% of the experimental finding for all three parameter sets, suggesting that cell morphology does not noticeably influence this response feature (Fig 3A). In contrast, the mean range of input resistance in our example sets represented ∼50% of the range observed in experiments, which indicates a high impact of morphological properties on the input resistance (Fig 3B). The range of

spike count values was 11 for the parameter set representing highly active T cells (set 1, green), 5 for the parameter set yielding medium spike activity (set 2, red), and 3 for the parameter set causing low activity (set 3, grey) (Fig 3C). Each of the parameter sets covered only a fraction of the experimentally observed range, which stretched from 2 to 28 spikes in response to 500 ms of current injection. This suggests that morphological variety within a cell population contributes to variability of spike counts, but not as much as biophysical differences do. The variability of the simulated first spike latencies corresponded to only ∼7% of the variability observed in experiments (Fig 3D). The height of the second spike was highly variable across reconstructed morphologies and covered ∼78% of the observed range in experimental data (Fig 3E). The repolarization duration was systematically above the experimentally observed median for all three parameter sets and covered on average 26% of the experimentally determined range (Fig 3F).

Fig 3. Variability in response features caused by morphological diversity with the same biophysical properties. Boxplots of response features of experimentally recorded T cells (n = 60, blue, re-plotted from Fig 2) and three example parameter sets (green, red and grey) applied to n = 15 different reconstructed morphologies. The range of each boxplot shows the variability in response features introduced by morphological details. The shown response features (with scaling as in Fig 2) are A) resting membrane potential, B) input resistance, C) spike count (in 500 ms), D) first spike latency E) spike height, F) repolarization period.

In summary, even when the same parameter set was applied to the population of 15 reconstructed morphologies, morphological details alone introduced considerable variability to the responses of T cell models. The strongest impact was observed in simulated input resistances and spike heights. Taken together, our results indicate that both biophysical diversity and morphological variation are needed to explain the range of response variance observed in T cells.

SIZ location influences spike features

Next, we analyzed the two morphological subtypes of T cells separately and investigated how the location of the SIZ influences the simulated response features. We tested six different SIZ configurations (configuration i-vi in Fig 4A-F) using example parameter set 2 (from Fig 2) and the reconstructed 1RP morphology presented in Fig 1A. In the standard configuration (configuration i in Fig 4A, which was also used in Figs. 1, 2 and 3), the SIZ with larger conductance density was located in the root process. The other configurations included relocating the SIZ to one of the other processes of the cell (Fig 4B-E), as well as distributing the total conductance of the standard configuration homogeneously over the simulated membrane (configuration vi in Fig 4F). All tested configurations generated spikes in response to somatic stimulation, although not all features remained within experimentally observed ranges. Compared to the standard configuration (i), spike counts can be higher or lower, depending on the SIZ location. The spike height measured in the soma differed as well between configurations. Spike amplitudes were larger when the SIZ was located in the main process (configuration ii, Fig 4B), or when the total conductance of the SIZ (Table 2) was distributed homogeneously across the entire cell membrane (vi) (Fig 4B and F).

Analyzing the impact of the SIZ location on response features for all reconstructed morphologies of our population, we found that the SIZ location has virtually no impact on the resting membrane potential or the input resistance of the simulated responses (not shown). For the spike features, the influence of the SIZ configuration was variable across the reconstructed morphologies. Figure 5 color-codes the differences between the

Fig 4. SIZ configuration in the same 1RP morphology influences spike responses. Example voltage traces measured in the soma compartment for six different SIZ configurations in the reconstructed 1RP morphology from Fig 1B. Conductance densities in the membrane of the reconstructed morphology are color coded with saturated colors indicating higher densities and areas of passive membrane shown less saturated (see colorbar). A) SIZ located in the root process to the skin is the standard 1RP SIZ configuration (i) used in this study. B) SIZ located in the main process (configuration ii, close to the soma) results in more and larger spikes in the soma. C) SIZ located in the process to the anterior ganglion (configuration iii) increases spike height and spike count slightly compared to standard configuration i. D) SIZ located in the central process (configuration iv) leads to a similar number of spikes with slightly increased height compared to configuration i. E) SIZ located in the process to the posterior ganglion (configuration v) elicits a similar spike count and spike height as the standard SIZ configuration i. F) Distributing the conductances of the SIZ section homogeneously over the whole membrane (configuration vi) causes larger spikes.

response feature values of each SIZ configuration (ii-vi: x-axes) and the standard configuration i for each reconstructed 1RP morphology in the population sorted by surface area (y-axes corresponding to numbers in S1 fig). The spike count increased in all reconstructed morphologies when the SIZ was located either in the main process (ii) or in the anterior process (iii), with morphologies with smaller total membrane surface showing the strongest effects. (Fig 5A). The strongest increase in spike count was observed for the reconstructed morphology 1 (the morphology with the smallest total surface area) in configuration ii, which responded with 24 additional spikes. When the SIZ was located in the central- or posterior process (configurations iv and v), only minor changes in the number of spikes were observed. When the total conductance was distributed homogeneously (vi), most reconstructed morphologies responded with more spikes compared to their standard configuration, except for the reconstructed morphology 4, which produced one spike less.This reconstructed morphology differs from the other members of the population in having a thick and long central process, while the other processes are rather thin (S1 Fig). The first spike latency decreased strongly for configurations ii and iii, in which the SIZ was located closer to the soma, as well as the homogeneous conductance distribution vi (Fig 5B). The latency of reconstructed morphology 1 reduced by 2.4 ms when the SIZ was located in the main process (configuration ii), making it faster than any experimentally observed T cell. As with spike count, configurations iv and v had only minor effects, producing slight decreases, no change, or, for the morphology with the largest surface, a negligible increase in latency. Spike height increased for all 1RP models when the SIZ was located in the main process (ii), in the anterior process (iii), or in the central process (iv) (Fig 5C). Reconstructed morphology 1 showed an increase of spike height by 48.23 mV for configuration ii, exceeding the experimentally observed spike height in our dataset. Placing the SIZ in the posterior process (v) yielded similar spike heights compared to the standard configuration. When conductance densities were distributed homogeneously (configuration vi), the spike height increased for all morphologies, similar to configuration ii. The impact of the SIZ location on the repolarization period was variable across reconstructions, but 7 out of 8 reconstructions showed shorter repolarization periods when the SIZ was located in the distal process (v), or when conductance densities were distributed homogeneously (vi). The highest increase of 0.9 ms was observed in reconstructed morphology 4 (with a large central process and thin other processes) in configuration iii and the largest decrease of -1 ms for morphology 8 (with the largest surface) in the homogeneous configuration vi.

For the population of seven 2RP T cells we assumed in the standard configuration (I

Fig 5. SIZ configuration influences spike response features in all reconstructed 1RP morphologies. Heatmaps of spike feature differences depending on the SIZ configuration (x-axes) for 8 reconstructed 1RP morphologies sorted from smallest surface area (1) to largest surface area (8) (y-axes), morphology 5 is the same as shown in Fig 4. Labels of SIZ configurations refer to those in Fig 4. Differences were calculated for each reconstructed morphology by subtracting the response feature value obtained for the standard SIZ configuration i (Fig 4A) from the value obtained for each SIZ configuration. Differences in A) spike counts, B) first spike latency, C) spike height, and D) repolarization duration are color coded with increases shown in red and decreases in blue (see colorbar).

in Fig 6A, also used in Figs 1 and 3) that they have two SIZs, one in each root process. This assumption is based on the findings of Meiser et al. [13], that 2RP cells have systematically higher spike counts and spike heights compared to 1RP cells, which lead to their hypothesis that 2RP cells have two SIZs, while 1 RP cells have only one SIZ. We tested six SIZ configurations for 2RP models with example parameter set 2 and one example reconstructed morphology (configuration I-VI in Fig 6A-F, same morphology as in Fig 1 and number 5 in S2 Fig) to investigate how the distribution of active membrane affects the response features of a 2RP T cell. In configuration II, we placed one SIZ in the anterior process and one in the posterior process, to separate them spatially as far as possible from each other, without changing the total conductance (Fig 6B). In this configuration, we observed higher spikes compared to the standard configuration I.

With configuration III, we challenged our assumption of 2RP T cells havening two SIZs. In this configuration, we omitted the SIZ from the proximal root process. This left the reconstructed morphology with approximately half the total conductance of standard configuration I for 2RP morphologies, and a similar amount to 1RP morphologies, which by definition have only one SIZ. This reduction of total conductances caused fewer and smaller spikes in the simulated responses for configuration III (Fig 6C) compared to the 2RP morphology in configuration I, and even compared to the standard configuration of the 1RP morphology (compare Fig 4A). When the total conductances from both SIZ in the standard configuration were combined in one SIZ in the distal root process (configuration IV), the simulated response was similar to the standard configuration, indicating that not the number of SIZs, but the total conductance determines the excitability (Fig 6D).

To investigate the impact of total conductances separately from morphological properties, we considered two configurations in which the total conductance of SIZs was distributed homogeneously across the membrane of the reconstructed morphology. In configuration V, we distributed the total conductance of the standard configuration I homogeneously over the cell membrane and observed more and larger spikes in the simulated response, compared to the standard configuration I (Fig 6E).

Lastly, we homogeneously distributed the total conductance of configuration III (only one SIZ) across the reconstructed morphology (configuration VI in Fig 6F), resulting in a homogeneous configuration with approximately half the total conductances compared to configuration V. For this homogeneous distribution of a lower total conductance (configuration VI), we observed fewer, but larger spikes compared to the responses of the standard configuration I and considerably fewer spikes than for configuration V with a homogeneous distribution of higher total conductance.

Analogue to the analysis of 1RP reconstructions, we calculated the difference between the response feature values of each SIZ configuration and the standard configuration I for each 2RP reconstructed morphology (Fig 7). Spike counts decreased in all reconstructed morphologies for the two configurations with lower total conductances, i.e. when the SIZ in the proximal root process was omitted to allow a

Fig 6. SIZ configuration in the same 2RP morphology influences spike responses. Voltage traces resulting from different SIZ configurations in an example reconstructed 2RP morphology, displayed as in Fig 4. A) Standard 2RP configuration: SIZs located in both processes to the skin. B) SIZs located in the anterior and posterior processes elicit a similar spike count and slightly higher spikes. C). Omitting the SIZ in the proximal process to the skin and keeping the SIZ in the other root process as in the standard configuration results in a reduced spike counts and smaller spikes compared to the standard configuration for 2RP (A), and also for 1RP (Fig 4A). D) Combining the conductance of both SIZ in the distal root process elicits a similar response to the standard configuration. E) Total conductance of configuration IV homogeneously distributed increases the spike count and spike height. F) Total conductance of configuration IV (approximately half of the total conductance compared to V) homogeneously distributed elicits fewer but higher spikes than the standard configuration I.

direct comparison to 1RP reconstructions (III) or when the conductance density of configuration III was distributed homogeneously in configuration VI (Fig 7A). When the conductance of the standard configuration I was distributed homogeneously (V), spike counts increased for all reconstructed morphologies, with a stronger impact on morphologies with smaller total surface. Placing SIZs in the anterior and posterior process (II) caused a slight increase of spike counts in two reconstructed morphologies and a slight decrease in two other reconstructed morphologies. When the conductance densities of both SIZs were combined in the distal root process (IV), responses were similar to the standard configuration I. First spike latency decreased in most reconstructed morphologies, when SIZs were located in the anterior and posterior process (II), and also when SIZ conductances of both SIZs were distributed homogeneously in configuration V (Fig 7B). Omitting one SIZ (III), or distributing the conductance of one SIZ homogeneously (VI) increased the first spike latency. Combining both SIZs in the distal root process (IV) led to similar first spike latencies compared to the standard configuration. The observed spike height decreased, when the SIZ in the proximal root process was omitted (III). This effect remained, when the conductance of both SIZ were combined in the distal root process in configuration IV (Fig 7C). Remarkably, the spike height increased compared to the standard configuration when the conductances of only one SIZ were distributed homogeneously (VI), although the total conductance was lower. Repolarization period became shorter for all configurations, except for configuration II where both SIZ were shifted to compartments that were further apart (Fig 7D).

Fig 7. SIZ configuration influences spike response features in all reconstructed 2RP morphologies. Heatmaps of differences in response feature values compared to the 2RP standard configuration I (Fig 6A) were calculated accordingly as in Fig 5 for 7 reconstructed morphologies with two root processes and sorted from smallest surface area (1) to largest surface area (7), morphology 5 is the same as shown in Fig 6. Labels of configurations on the y-axis refer to those in Figure 6. Differences in A) spike counts, B) first spike latency, C) spike height, and D) repolarization duration are color coded with increases shown in red and decreases in blue.

By testing different SIZ configurations for both morphological subtypes we found that they did not impact the passive response features (input resistance and resting potential), but strongly influenced all spike features. It should be kept in mind that the parameter sweep was performed based on the assumption of the standard SIZ

configurations and therefore combined eight 1RP reconstructed morphology with one SIZ and seven 2RP reconstructed morphologies with two SIZ. Our results show for one example parameter set that biologically plausible responses do not critically depend on this experimentally not testable assumption, but can qualitatively also be obtained with other SIZ configurations, although all spike response feature values depend quantitatively on the SIZ configuration (Fig 5 and 7).

Systematical differences between morphological subtypes can be explained by total conductance of active membrane

In our exploration of the parameter space, we assumed one SIZ for T cells with 1RP morphology and two SIZs for the 2RP morphological subtype as standard configurations. Therefore, it is important to determine whether differences in morphology or in total conductance can explain the higher activity of the 2RP morphological subtype observed in experiments.

In the strip plots of Figure 8, the experimental data set from Figure 2 is compared to the simulation results obtained for the three parameter sets of figure 3 applied to the eight 1RP and the seven 2RP reconstructed morphologies. All three example parameter sets showed the same trends: The 2RP morphologies in the standard configuration I generate more and higher spikes than the 1RP morphologies in standard configuration i when the same parameter set is applied (compare same colors in Fig 8A). This result is consistent with the experimental findings by Meiser et al. [13], but depends critically on the assumed SIZ configurations. For most neuronal types, it is assumed that they have only one SIZ, usually located at their axon initial segment [39]. When assuming that also all leech T cells, independent of their number of root processes, posses only one SIZ with the same conductance density, (comparison of configurations i and III), the spike counts of the 2RP models fall below the spike counts of 1RP models with the same parameter set. Combining conductance densities from both SIZs into the distal root process (configuration IV), 2RP models respond with spike counts similar to their standard configuration I. These findings imply that it is very likely for T cells with two root processes to possess a higher total conductance than the morphological subtype with one root process to explain the experimentally found higher number of spikes in the 2RP morphological subtype of T cells.

In an experimental study [13], first spike latencies were reported to be shorter for the 2RP morphological subtype. In our small samples of reconstructed morphologies, we did not observe a consistent latency difference between 1RP and 2RP models under their standard SIZ configurations (Fig 8B). However, when the SIZ in the proximal root process was omitted in configuration III, the latency increased beyond the values observed for the 1RP models, which would contradict the experimental findings. This latency increase was due to the lower total conductance, as can be seen from the comparison with configuration IV, in which the standard total conductance condensed into one SIZ leads to approximately the same latencies as observed for the standard configuration I (Fig 8B).

Spike height was systematically larger for 2RP morphologies in configurations I and IV compared to 1RP morphologies (Fig 8C). When the proximal SIZ was omitted, which reduced the total conductance (configuration III), 2RP spike heights decreased to the 1RP level. In configuration IV, condensing the total conductance of configuration I into one SIZ increased spike height relative to configuration III, but values remained below those of the standard 2RP configuration I. These findings also indicate that also the experimentally found differences in spike height [13] depend strongly on the total conductance. The repolarization periods, which were not investigated in the experimental study [13], followed the trends observed for spike heights and spike counts

(Fig 8D).

These results indicate that the previously reported differences in spike counts and spike heights between 1RP and 2RP T cells cannot be explained by morphology alone, but instead require differences in total conductance. Assuming approximately the same total conductance for both morphological subtypes leads to results that contradict the experimental findings. While our model study clearly shows the importance of a higher total conductance in the 2RP morphological subtype, it is still unanswered if the total conductance is distributed to two separate SIZ located within the central ganglion, since other SIZ configurations lead to similar results.

Fig 8. Systematic differences in spike responses between reconstructed 1RP and 2RP morphologies. Strip plots of spike response features of n = 60 experimentally recorded neurons (blue, same data as in Fig 2 and 3), and three example parameter sets (green, red and grey, same parameter sets as in Fig 3) applied to n = 8 one root process morphologies with an SIZ located in their root process (see Fig 4A, standard configuration i, and S1 Fig for reconstructed morphologies) and n = 7 two root process morphologies with two SIZs in each root process (see Fig 6A, standard configuration I, and S2 Fig for reconstructed morphologies). Additionally, response features for the 2RP morphologies are shown for SIZ configurations III (one SIZ with half total conductance, Fig 6C) and IV (one SIZ with full total conductance, Fig 6D). For each SIZ configuration, the color indicates the applied parameter set. Strip plots for A) spike counts, B) first spike latency, C) spike height and D) repolarization period.

Discussion

Understanding the sources of variability in neuronal responses remains a fundamental challenge in neuroscience. This study demonstrated that variability in morphological details, even within the same cell type and fixed arborization pattern, does impact neuronal response features. Using a large database of parameter sets that generated biologically plausible leech T cell responses across 15 reconstructed morphologies (Fig 2), we demonstrated that differences in morphological details like diameters and length of cellular sections induce variability in T cell responses (Fig 3). Our results indicate that previously reported typical responses of 1RP and 2RP T cells [13], can arise from different SIZ configurations (Fig 4 and 6). We also found that the distribution of ion channels in the neuronal membrane has an impact on spike features (Fig 5 and 7). Our approach also offers an explanation for the systematic differences which may be driven by differences in SIZ properties between the two morphological subtypes of 1RP and 2RP (Fig 8).

The interplay of morphological details, biophysical diversity and channel distribution as sources of variability

Our study focused on the influence of biophysical and morphological diversity on two subthreshold response features and four spike response features of leech T cells. Changes in SIZ configuration had virtually no effect on input resistance, whereas varying biophysical properties or introducing morphological diversity produced considerable variability. Resting membrane potentials in the simulations were less variable than in experiments, suggesting that they are only weakly influenced by biophysical or morphological variability or by SIZ configuration. However, it should be noted that the range of experimentally observed resting membrane potentials in this data set is larger than in previous studies on T cells [38, 40]. It is likely that the process

of impaling the cell membrane during the intracellular recording impacts the resting membrane potential during experiments, and therefore the experimental data may overestimate the variability of the resting membrane potential compared to unperturbed T cells. Additionally, the variability in simulated resting potentials is likely underestimated, since the membrane capacitance C_m and the axial resistance R_i were not varied in this study.

Spike features showed different dependencies on the three factors of variability, biophysical diversity, differences in morphological details and location of the SIZ. Biophysical diversity caused variable spike counts, as reported in previous studies [23, 41], but did not make the example reconstructed morphology in Fig 2 a very active T cell. However, high spike counts were found for other morphologies in the population of simulated T cells (Fig 3C). This confirms that morphological details are an important factor in neuronal excitability. The location of the SIZ also influenced the spike count strongly, suggesting that the exact location of the SIZ might be variable from T cell to T cell. First spike latency showed little variability between different biophysical parameter sets, or between reconstructed morphologies. The SIZ configuration, however, strongly affected the first spike latency, especially in reconstructions with a smaller surface area (Fig 5B and Fig 7B). This is in line with findings of a previous modeling study, reporting that spike latency of vertebrate neurons is mostly influenced by cell size and SIZ location [42]. Spike timing carries a lot of information in mechanosensation [43], and therefore our results underline the crucial role of SIZ location in T cells, and may also apply in other mechanoreceptors. Spike height was very variable when one parameter set was applied to the population of reconstructed morphologies and when the SIZ location was varied, while it was less strongly impacted by the biophysical parameters. We found variable repolarization periods for all three factors we investigated, but the repolarization period was systematically above the median value of experimentally observed responses. For homogeneously distributed ion channel conductances, we found shorter repolarization periods in almost all morphological reconstructions. This could indicate that we underestimated the ion-channel conductances in the passive compartments. Another possible factor that could influence the repolarization period as well as the other spike features is the ion channel kinetics [19, 44, 45], which were not varied in this study, but only approximated based on a patch clamp recording (S3 Fig).

Our results agree with the findings of prior studies on degeneracy in neural systems that many distinct parameter combinations can produce functionally equivalent outputs [14–16]. We identified 33,958 parameter sets that generated responses resembling T cells for 15 reconstructed morphologies. Morphological properties such as the soma size and location, dendritic arborization and axonal properties are known to shape neural response features [46–48]. Our results reveal that morphological details alone can give rise to variability in response features such as input resistance, spike count, and spike height, even when all biophysical parameters and the overall arborization pattern are held constant. These findings suggest that even minor morphological differences, such as the diameter and length of a dendritic branch, contribute to the response variability of T cells and likely to neuronal response variability in general. This, in turn, may contribute to variability at the network level [49]. Moreover, our approach likely underestimated the impact of morphology, since we used simplified reconstructions of morphologies and therefore did not take the fine arborization into consideration, which is also a known source of variability [12, 50].

It is clear that there are more sources of neuronal response variability than morphological details, the biophysical parameters of conductances, and the density and spatial distribution of ion-channels, which we considered in this study. Other factors including the ion channel dynamics [45], chemical synaptic [7] and electrical coupling

between cells [51] are also known to contribute to neuronal variability. Further studies should determine how all of these mechanisms interact to give rise to robust networks and facilitate many possible solutions for functional output.

Systematic differences between subtypes of a defined cell type

Understanding how morphological properties influence neuronal responses is a crucial task in computational neuroscience, especially for classifying and understanding the function of subtypes of neuronal cell types [11, 12, 28, 52–54].

Leech T cells are a well-studied and experimentally accessible example of neurons with two morphological subtypes. All T cells are mechanoreceptors, which respond to light touch on the skin. Previous experimental and modeling studies suggested that all T cells require at least two SIZs to reliably transmit signals from the skin to the central part of the ganglion: a peripheral SIZ is located in the skin, and a central SIZ is located close to the ganglion [36, 37]. Here, we simulated a T cell in an isolated ganglion, neglecting the distal processes that innervate the skin with the peripheral SIZ. Unfortunately, experimental limitations do not allow us to measure ion channel distribution on the membrane of T cells and therefore prevent the exact SIZ location from being determined. The electrophysiological recordings allow only indirect reasoning: Since the first spike in response to current injection into the soma occurs at a median latency of 7 ms, the SIZ is likely not close to the soma. This argument is supported by a previous model study, in which a single compartment model failed to reproduce the T cell response latency [38]. Our simulation result for the 1RP morphological subtype points in the same direction. When the SIZ was located directly next to the soma in the main process, the simulated latencies were shorter than those observed in experiments (Fig 5B). Nevertheless, since several different configurations of channel distributions, including SIZ locations in different segments, as well as homogeneously distributed ion channels, reproduce biologically plausible responses, our approach was unable to determine the location of the SIZ in biological T cells. Our results indicate that the location of the central SIZ is important for spike timing and other spike response features. but may vary from cell to cell. It is also possible that the location of the SIZ in T cells might change dynamically and thereby contribute to homeostatic plasticity, a mechanism proposed by prior studies to regulate excitability of cells in response to sensory or synaptic input [55–57].

In this study, we compared two morphological subtypes, which are known to differ also in function. In each ganglion, two T cells of the 1RP morphological subtype innervate the dorsal region of the leech skin, while the other four T cells possess a 2RP morphology and respond to touch on the ventral or lateral skin regions [33]. The distribution of ion channels across the membrane is even more unclear for the 2RP than for the 1RP morphological subtype. Since both root processes reach the skin at different positions, it is safe to assume that both of them possess a peripheral SIZ that send action potentials towards the ganglion when the respective skin area is stimulated. It is unknown if this morphological subtype also posses two central SIZ. But our simulations show that the experimental observation that T cells with two root processes exhibited higher spike counts and greater spike amplitudes than their one-root counterparts [13] can only be explained by a higher total conductance in the 2RP morphological subtype. If the same total conductance is assumed in both subtypes, the larger membrane area of the additional root process reduces the excitability of 2RP models, so that they produce fewer instead of more spikes than the 1RP models. Hence, the 2RP morphological subtype must possess more ion channels, but our model approach does not allow a conclusion if these are located in one more densely populated SIZ, located in two SIZ, or distributed across a larger membrane area.

Through the manipulation of SIZ properties and locations, we showed that increased

active membrane area and proximity to the soma can enhance excitability. This finding suggests an interplay between morphology and biophysical properties that explains subtype-specific functional differences. This supports the hypothesis that additional SIZs in the root processes could contribute to the systematic differences between T cell subtype responses. Our results reveal how morphology, ion channel distribution, and electrical properties interact to generate variability in neuronal responses, highlighting multiple pathways by which the nervous system achieves reliable function.

Materials and methods

We wrote custom software in Python 3.9.13 for data analysis and simulations. T cell models were designed using Brian 2, version 2.5.4 [58]. All the data and software can be found in our gin-gnode repository (`https://gin.g-node.org/Strandpalme/Sandbote_et_al_2025_plos_computational_biology` a DOI will be requested).

Data analysis of electrophysiological data

Data from **N=60** cells of the previously published T cell dataset from Meiser et al. [13] were reanalyzed. The test protocol was 11 s long and consisted of a -1.5 nA pulse for 500 ms starting at 4 s and a 1.5 nA pulse for 500 ms starting at 8.5 s (Fig 1C). We only considered the second spike of the response for spike shape features, because the shape of the first spike differs systematically from subsequent spikes. Therefore, we excluded all cell responses with a spike count of 1. We analyzed the following response features:

- **Resting membrane potential** [mV] was determined as the median membrane potential over 500 ms before the first stimulation.
- **Input resistance** [MΩ] was calculated as follows:

$$R_I = \frac{V_{hyp} - V_{rest}}{I_{stim}} \tag{1}$$

  with R_I as the input resistance, V_{hyp} as the median membrane potential during a 500 ms hyperpolarizing current pulse of $I_{stim} = -1.5$ nA and V_{rest} beeing the resting membrane potential.
- **Spike count** was defined as the number of action potentials in response to a 500 ms depolarizing current injection of +1.5 nA.
- **Latency** was determined as the time difference between the stimulus onset of the +1.5 nA current injection and the peak of the first spike.
- **Spike height** was measuered as the absolute voltage difference between the peak of the second spike in response to current injection of +1.5 nA and the minimum of the respective afterhyperpolarization within a time window of 10 ms.
- **Repolarization duration** was defined as the time difference between the peak of the second spike in response to +1.5 nA current injection and the minimum of the respective afterhyperpolarization.

Morphological reconstruction

We used 15 of the anatomical reconstructions previously published by Meiser et al. [13]. Eight were reconstructions of T cells with one root process, and 7 were T cells with two root processes. The comparison between the microscopy pictures and the corresponding

reconstructed morphologies is shown for two examples in Fig 1. The supplementary figures S1 Fig and S2 Fig display all 15 reconstructed morphologies, and indicate the diameters of their compartments. We applied a Ramer-Douglas-Peucker algorithm to all reconstructions to simplify structures equally and reduce variability in the number of compartments between cells [59]. We set the distance tolerance ϵ to 1 µm in the algorithm for all morphologies, resulting in a median of 120 compartments for one-root-process reconstructions and a median of 162 compartments for two root process models. To reduce methodological variability of morphologies, the minimum distance from the tip of the anterior process to the soma were determined and the anterior process of all morphologies were cut to match this value for all morphologies (see magenta lines in Fig1A and E). The same procedure was applied to the posterior process. Root processes were also cut to the shortest length found in the population to ensure same length in all morphologies.

Multi-compartment model

We reproduced electrical T-cell responses with a conductance based multi-compartmental model. The dynamics of the membrane voltage in each compartment was calculated as follows:

$$C_m \frac{dV}{dt} = I_{K_f} + I_{K_s} + I_{Na} + I_M + I_L \tag{2}$$

With $C_m = 1\ \mu F/cm^2$ as the standard membrane capacitance, V is the membrane voltage at time point t and I_x describes the transmembrane current for each current type. Compartments were connected by an intracellular resistance of $R_i = 100\ \Omega\ cm$, as in previous studies [60]. Voltage clamp experiments of our lab revealed fast and slow components in the K^+ current (S3 Fig), so we added corresponding ion-channels in our model. Due to the large size of leech cells, only a rough estimation of the ion-channel kinetics was possible, which was used as a starting point for hand tuning of ion channel kinetics. For the fast K^+ current, we implemented a Shaw-like Kv3.1 channel which is often expressed in cells that generate rapid trains of action potentials [61]. Channels of this type were also identified in the transcriptome of *H. verbana* [62]. We formalized the current of the fast potassium channel as follows:

$$I_{K_f} = g_{K_f} \cdot n_f^4 \cdot p \cdot (E_K - V) \tag{3}$$

With g_{K_f} as the conductance density of the fast potassium channel, n_f and p are the gating variables, E_K is the reversal potential of K^+ and V is the membrane potential. For the slow potassium current we defined:

$$I_{K_s} = g_{K_s} \cdot n_s \cdot (E_K - V) \tag{4}$$

With g_{K_s} as the conductance density for the slow potassium channel and n_s is the gating variable. The fast transient sodium channel [63] was formulated as:

$$I_{Na} = g_{Na} \cdot m^4 \cdot h \cdot (E_{Na} - V) \tag{5}$$

where g_{Na} is the conductance density for Na^+-ions, m and h are the gating variables, E_{Na} is the reversal potential of Na^+ and V is the membrane potential. An M-type potassium channel was added to cease spiking during current injection [38, 64]. It was formulated as:

$$I_M = g_M \cdot z^2 \cdot (E_K - V) \tag{6}$$

With g_m as the maximum conductance of the M-type channel and z as the gating variable. Kinetic equations for the slow and fast potassium channel where formulated as:

$$\frac{dx(t)}{dt} = \frac{x_\infty(V) - x}{\tau_x} \tag{7}$$

Where x is either n_f, n_s, p, m, h, or z, x_∞ corresponds to the respective steady state value and τ_x is the respective time constant (Table 1). The steady state functions where defined by:

$$x_\infty = \frac{1}{1 + e^{(-\frac{v+x_1}{x_2})}} \tag{8}$$

For the sodium and M-type potassium current, τ_x was voltage dependent and was calculated as:

$$\tau_x(V) = T_x \cdot \left(\frac{2}{e^{(-\frac{V+x_1}{x_2})} + e^{(\frac{V+x_1}{x_2})}} \right) \tag{9}$$

Table 1. Constant parameter values of ion-channel kinetics

Current	Parameter	Value	Equation
I_{K_f}	$n_{f_1};\ n_{f_2}\ [mV]$	1; 16.5	8, 9
I_{K_f}	$p_1;\ p_2\ [mV]$	15; 8	8, 9
I_{K_f}	$T_{n_f}\ [ms]$	1	9
I_{K_s}	$n_{s_1};\ n_{s_2}\ [mV]$	25; 19.19	8, 9
I_{K_s}	$T_{n_s}\ [ms]$	67.18	9
I_M	$z_1;\ z_2\ [mV]$	40.76; 2.62	8, 9
I_M	$T_z\ [ms]$	94.03	9
I_{Na}	$m_1;\ m_2\ [mV]$	20; 11	8, 9
I_{Na}	$h_1;\ h_2\ [mV]$	28; 10.35	8, 9
I_{Na}	$T_m\ [ms]$	0.8	9
I_{Na}	$T_h\ [ms]$	19.25	9

Table 2. Ranges of varied parameters

	parameter ranges			example parameters		
Parameter	min	max	step	set 1	set 2	set 3
$E_K\ [mV]$	-80	-40	10	-50	-60	-50
$E_{Na}\ [mV]$	20	60	10	40	30	60
$E_L\ [mV]$	-60	0	15	-45	-45	-30
$g_{K_f}\ [mS/cm^2]$	250	1250	250	500	750	500
$g_{K_f}(SIZ)\ [mS/cm^2]$	600	1140	180	600	960	960
$g_{K_s}\ [mS/cm^2]$	0.01	0.09	0.02	0.09	0.03	0.07
$g_{Na}\ [mS/cm^2]$	7	11	1	7	8	7
$g_{Na}(SIZ)\ [mS/cm2]$	140	380	60	140	200	140
$g_M\ [mS/cm^2]$	1	5	1	1	1	3
$g_M(SIZ)\ [mS/cm2]$	0.1	1.7	0.4	0.1	0.5	0.1
$g_L\ [mS/cm^2]$	0.02	0.1	0.02	0.1	0.1	0.08

We chose 5 values for each varied parameter, resulting in $5^{11} = 48.828.125$ combinations.

Spike initiation zone configuration

The SIZ had higher conductance densities for g_{K_f}, g_M and g_{Na} (see model section), compared to the other sections. In the standard configuration, the SIZ was located in the root process of the 1RP morphologies. For the 2RP morphologies, both root processes contained a SIZ with the same conductance density. Hence, the total conductance was higher in the standard configuration of 2RP than of 1 RP morphologies. For the homogeneous configurations vi and V (Fig 4F and Fig 6E) we calculated the total conductance of g_{K_f}, g_M and g_{Na} in the standard configuration and distributed it homogeneously over the membrane surface. For the homogeneous configuration VI (Fig 6F), we used configuration III and distributed its total conductance homogeneously.

Parameter study

We simulated responses to a shortened stimulation protocol for somatic current injection. We applied the same stimulus as described above for experimental data. To evaluate the response for a given parameter set, we compared each response feature to the corresponding experimentally derived data. A simulated response was considered valid if the following inequation was true for all analyzed response features:

$$min(x_i) < \tilde{x}_i < max(x_i) \tag{10}$$

with $max(x_i)$ and $min(x_i)$ as the maximum respectively the minimum of the experimentally measuered response feature values and $\tilde{x}_i$ as the corresponding response feature value in the simulated response.

Using the Python package psweep, we created a parameter grid with all possible combinations of the given parameters (Table 2). The sweeps were parallelized on the HPC cluster of the University of Oldenburg, utilizing the Dask Python package [65]. The parameter sweeps were done in two steps: **1**: All combinations of the parameters in Table 2 were applied to one T-cell morphology with one branch. The simulated responses were compared to the experimentally observed responses concerning the response features listed above. **2**: The parameter combinations that yielded valid responses for the selected example anatomy were tested on the entire population of morphologies. In this parameter search, a parameter set was considered valid if inequation 10 was true for all morphologies. For the examples presented in the "Many Parameter Sets Reproduce T-Cell Responses" section, we decided to show a morphology with response feature values at the center of the response feature distribution for the entire population. For the example simulations in the "Results" section, we randomly selected three parameter sets that yielded different spike counts, mimicking highly, medium and less active T cells in our data set (Table 2).

Supporting information

S1 Fig. Reconstructed 1RP morphologies. All reconstructed 1RP morphologies used in this study, sorted by total membrane surface to match labeling in Fig 5. Gray lines indicate the skeleton of the reconstruction, the orange dots indicate the center and diameter of individual compartments.

S2 Fig. Reconstructed 2RP morphologies. All reconstructed 2RP morphologies used in this study, sorted by total membrane surface to match labeling in Fig 7. Gray lines indicate the skeleton of the reconstruction, the orange dots indicate the center and diameter of individual compartments. Reconstruction 5 was used as an example

S3 Fig. Patch-clamp recording of potassium currents in a leech Touch cell in sodium-free solution. Potassium currents were isolated by using a sodium-free solution. The top panel shows outward K^+ currents, each trace corresponding to a voltage-step protocol shown in the bottom panel. The cell was held at –90 mV, and depolarizing steps were applied in 5 mV increments up to +75 mV. At low voltages, the K^+ current exhibits a slow component that dominates throughout the 100 ms stimulation. With increasing depolarization, a fast-activating component emerges at the onset of the voltage step. Due to the large size of the T cell, complete space clamp could not be achieved, which limits the voltage control to the soma and proximal neurite. Therefore, the recordings represent an approximate measure of somatic and primary neurite potassium currents.

Acknowledgments

We thank the division for computational neuroscience and especially Dr. Go Ashida, Daniela Antonia Schwarz, Austin McNamara and Brittni Paige Devlin for valuable discussion and feedback on the manuscript.

References

1. Brette R. Brains as computers: Metaphor, analogy, theory or fact? Frontiers in Ecology and Evolution. 2022;Volume 10 - 2022. doi:10.3389/fevo.2022.878729.

2. Rathour RK, Narayanan R. Degeneracy in hippocampal physiology and plasticity. Hippocampus. 2019;29(10):980–1022. doi:https://doi.org/10.1002/hipo.23139.

3. Linneweber GA, Andriatsilavo M, Dutta SB, Bengochea M, Hellbruegge L, Liu G, et al. A neurodevelopmental origin of behavioral individuality in the Drosophila visual system. Science. 2020;367(6482):1112–1119. doi:10.1126/science.aaw7182.

4. Bucher D, Prinz AA, Marder E. Animal-to-animal variability in motor pattern production in adults and during growth. Journal of Neuroscience. 2005;25(7):1611–1619. doi:10.1523/JNEUROSCI.3679-04.2005.

5. Calabrese RL, Norris BJ, Wenning A, Wright TM. Coping with variability in small neuronal networks. Integrative and Comparative Biology. 2011;51(6):845–855. doi:10.1093/icb/icr074.

6. Norris BJ, Wenning A, Wright TM, Calabrese RL. Constancy and variability in the output of a central pattern generator. Journal of Neuroscience. 2011;31(12):4663–4674. doi:10.1523/JNEUROSCI.5072-10.2011.

7. Roffman RC, Norris BJ, Calabrese RL. Animal-to-animal variability of connection strength in the leech heartbeat central pattern generator. Journal of Neurophysiology. 2012;107(6):1681–1693. doi:10.1152/jn.00903.2011.

8. Wenning A, Norris BJ, Günay C, Kueh D, Calabrese RL. Output variability across animals and levels in a motor system. eLife. 2018;7:e31123. doi:10.7554/eLife.31123.

9. Scherer JS, Riedesel OE, Arkhypchuk I, Meiser S, Kretzberg J. Initial Variability and Time-Dependent Changes of Neuronal Response Features Are Cell-Type-Specific. Frontiers in Cellular Neuroscience. 2022;Volume 16 - 2022. doi:10.3389/fncel.2022.858221.

10. Goodman CS. Isogenic grasshoppers: Genetic variability in the morphology of identified neurons. Journal of Comparative Neurology. 1978;182(4):681–705. doi:https://doi.org/10.1002/cne.901820408.

11. Moubarak E, Inglebert Y, Tell F, Goaillard JM. Morphological determinants of cell-to-cell variations in action potential dynamics in Substantia Nigra dopaminergic neurons. Journal of Neuroscience. 2022;42(40):7530–7546. doi:10.1523/JNEUROSCI.2331-21.2022.

12. Peng H, Xie P, Liu L, Kuang X, Wang Y, Qu L, et al. Morphological diversity of single neurons in molecularly defined cell types. Nature. 2021;598(7879):174–181. doi:https://doi.org/10.1038/s41586-021-03941-1.

13. Meiser S, Sleeboom JM, Arkhypchuk I, Sandbote K, Kretzberg J. Cell anatomy and network input explain differences within but not between leech touch cells at two different locations. Frontiers in Cellular Neuroscience. 2023;17: 1186997. doi:10.3389/fncel.2023.1186997.

14. Prinz AA, Bucher D, Marder E. Similar network activity from disparate circuit parameters. Nature neuroscience. 2004;7(12):1345–1352. doi:10.1038/nn1352.

15. Achard P, De Schutter E. Complex parameter Landscape for a complex neuron model. PLOS Computational Biology. 2006;2(7):1–11. doi:10.1371/journal.pcbi.0020094.

16. Alonso LM, Marder E. Visualization of currents in neural models with similar behavior and different conductance densities. eLife. 2019;8:e42722. doi:10.7554/eLife.42722.

17. Edelman GM, Gally JA. Degeneracy and complexity in biological systems. Proceedings of the National Academy of Sciences. 2001;98(24):13763–13768. doi:10.1073/pnas.231499798.

18. Goaillard JM, Marder E. Ion channel degeneracy, variability, and covariation in neuron and circuit resilience. Annual Review of Neuroscience. 2021;44:335–357. doi:https://doi.org/10.1146/annurev-neuro-092920-121538.

19. Schneider M, Bird AD, Gidon A, Triesch J, Jedlicka P, Cuntz H. Biological complexity facilitates tuning of the neuronal parameter space. PLOS Computational Biology. 2023;19(7):1–24. doi:10.1371/journal.pcbi.1011212.

20. Hodgkin AL, Huxley AF. A quantitative description of membrane current and its application to conduction and excitation in nerve. The Journal of physiology. 1952;117(4):500–544. doi:https://doi.org/10.1007/BF02459568.

21. Almog M, Korngreen A. Is realistic neuronal modeling realistic? Journal of Neurophysiology. 2016;116(5):2180–2209. doi:10.1152/jn.00360.2016.

22. Prinz AA, Billimoria CP, Marder E. Alternative to hand-tuning conductance-based models: Construction and analysis of databases of model neurons. Journal of Neurophysiology. 2003;90(6):3998–4015. doi:10.1152/jn.00641.2003.

23. Günay C, Edgerton JR, Jaeger D. Channel density distributions explain spiking variability in the globus pallidus: A combined physiology and computer simulation database approach. Journal of Neuroscience. 2008;28(30):7476–7491. doi:10.1523/JNEUROSCI.4198-07.2008.

24. Marder E, Taylor AL. Multiple models to capture the variability in biological neurons and networks. Nature Neuroscience. 2011;14(2):133–138. doi:https://doi.org/10.1038/nn.2735.

25. Jedlicka P, Bird AD, Cuntz H. Pareto optimality, economy–effectiveness trade-offs and ion channel degeneracy: improving population modelling for single neurons. Open Biology. 2022;12(7):220073. doi:10.1098/rsob.220073.

26. Eyal G, Mansvelder HD, de Kock CPJ, Segev I. Dendrites impact the encoding capabilities of the axon. Journal of Neuroscience. 2014;34(24):8063–8071. doi:10.1523/JNEUROSCI.5431-13.2014.

27. Goaillard JM, Moubarak E, Tapia M, Tell F. Diversity of axonal and dendritic contributions to neuronal output. Frontiers in Cellular Neuroscience. 2020;Volume 13 - 2019. doi:10.3389/fncel.2019.00570.

28. Kole MH, Brette R. The electrical significance of axon location diversity. Current Opinion in Neurobiology. 2018;51:52–59. doi:https://doi.org/10.1016/j.conb.2018.02.016.

29. Mainen ZF, Sejnowski TJ. Influence of dendritic structure on firing pattern in model neocortical neurons. Nature. 1996;382(6589):363–366. doi:10.1038/382363a0.

30. Kristan WB, Calabrese RL, Friesen WO. Neuronal control of leech behavior. Progress in Neurobiology. 2005;76(5):279–327. doi:https://doi.org/10.1016/j.pneurobio.2005.09.004.

31. Pirschel F, Kretzberg J. Multiplexed population coding of stimulus properties by leech mechanosensory cells. Journal of Neuroscience. 2016;36(13):3636–3647. doi:10.1523/JNEUROSCI.1753-15.2016.

32. Scherer JS, Sandbote K, Schultze BL, Kretzberg J. Synaptic input and temperature influence sensory coding in a mechanoreceptor. Frontiers in Cellular Neuroscience. 2023;17: 1233730. doi:10.3389/fncel.2023.1233730.

33. Nicholls JG, Baylor DA. Specific modalities and receptive fields of sensory neurons in CNS of the leech. Journal of Neurophysiology. 1968;31(5):740–756. doi:10.1152/jn.1968.31.5.740.

34. Meeks JP, Mennerick S. Action potential initiation and propagation in CA3 pyramidal axons. Journal of Neurophysiology. 2007;97(5):3460–3472. doi:10.1152/jn.01288.2006.

35. Guo Y, Liu Z, Chen Yk, Chai Z, Zhou C, Zhang Y. Neurons with multiple axons have functional axon initial segments. Neuroscience bulletin. 2017;33(6):641–652. doi:10.1007/s12264-017-0169-3.

36. Burgin A, Szczupak L. Network interactions among sensory neurons in the leech. Journal of Comparative Physiology A. 2003;189(1):59–67. doi:10.1007/s00359-002-0377-8.

37. Kretzberg J, Kretschmer F, Marin-Burgin A. Effects of multiple spike-initiation zones in touch sensory cells of the leech. Neurocomputing. 2007;70(10):1645–1651. doi:https://doi.org/10.1016/j.neucom.2006.10.048.

38. Meiser S, Ashida G, Kretzberg J. Non-synaptic plasticity in leech touch cells. Frontiers in Physiology. 2019;10: 01444. doi:10.3389/fphys.2019.01444.

39. Huang CYM, Rasband MN. Axon initial segments: structure, function, and disease. Annals of the New York Academy of Sciences. 2018;1420(1):46–61. doi:https://doi.org/10.1111/nyas.13718.

40. Scherer JS, Riedesel OE, Arkhypchuk I, Meiser S, Kretzberg J. Initial variability and time-dependent changes of neuronal response features are cell-type-specific. Frontiers in Cellular Neuroscience. 2022;16: 858221. doi:10.3389/fncel.2022.858221.

41. Berger SD, Crook SM. Modeling the Influence of Ion Channels on Neuron Dynamics in Drosophila. Frontiers in Computational Neuroscience. 2015;Volume 9 - 2015. doi:10.3389/fncom.2015.00139.

42. Gulledge AT, Bravo JJ. Neuron Morphology Influences Axon Initial Segment Plasticity. eNeuro. 2016;3(1). doi:10.1523/ENEURO.0085-15.2016.

43. Johansson RS, Birznieks I. First spikes in ensembles of human tactile afferents code complex spatial fingertip events. Nature neuroscience. 2004;7(2):170–177. doi:10.1038/nn1177.

44. Kole MH, Letzkus JJ, Stuart GJ. Axon initial segment Kv1 channels control axonal action potential waveform and synaptic efficacy. Neuron. 2007;55(4):633–647. doi:10.1016/j.neuron.2007.07.031.

45. Goaillard JM, Marder E. Ion Channel Degeneracy, Variability, and Covariation in Neuron and Circuit Resilience. Annual Review of Neuroscience. 2021;44(Volume 44, 2021):335–357. doi:https://doi.org/10.1146/annurev-neuro-092920-121538.

46. Hesse J, Schreiber S. Externalization of neuronal somata as an evolutionary strategy for energy economization. Current Biology. 2015;25(8):R324–R325. doi:10.1016/j.cub.2015.02.024.

47. Fékété A, Ankri N, Brette R, Debanne D. Neural excitability increases with axonal resistance between soma and axon initial segment. Proceedings of the National Academy of Sciences. 2021;118(33):e2102217118. doi:10.1073/pnas.2102217118.

48. Brette R. Sharpness of spike initiation in neurons explained by compartmentalization. PLOS Computational Biology. 2013;9(12):1–10. doi:10.1371/journal.pcbi.1003338.

49. Gowers RP, Schreiber S. How neuronal morphology impacts the synchronisation state of neuronal networks. PLOS Computational Biology. 2024;20(3):1–27. doi:10.1371/journal.pcbi.1011874.

50. Cuntz H, Forstner F, Borst A, Häusser M. One rule to grow them all: A general theory of neuronal branching and its practical application. PLOS Computational Biology. 2010;6:1–14. doi:10.1371/journal.pcbi.1000877.

51. Crodelle J, Zhou D, Kovačič G, Cai D. A Role for Electrotonic Coupling Between Cortical Pyramidal Cells. Frontiers in Computational Neuroscience. 2019;Volume 13 - 2019. doi:10.3389/fncom.2019.00033.

52. Mao X, Staiger JF. Multimodal cortical neuronal cell type classification. Pflügers Archiv-European Journal of Physiology. 2024;476(5):721–733. doi:10.1007/s00424-024-02923-2.

53. Chand AN, Galliano E, Chesters RA, Grubb MS. A Distinct Subtype of Dopaminergic Interneuron Displays Inverted Structural Plasticity at the Axon Initial Segment. Journal of Neuroscience. 2015;35(4):1573–1590. doi:10.1523/JNEUROSCI.3515-14.2015.

54. Scala F, Kobak D, Bernabucci M, Bernaerts Y, Cadwell CR, Castro JR, et al. Phenotypic variation of transcriptomic cell types in mouse motor cortex. Nature. 2021;598(7879):144–150. doi:10.1038/s41586-020-2907-3.

55. Goldstein RH, Barkai O, Íñigo-Portugués A, Katz B, Lev S, Binshtok AM. Location and plasticity of the sodium spike initiation zone in nociceptive terminals in vivo. Neuron. 2019;102(4):801–812. doi:10.1016/j.neuron.2019.03.005.

56. Grubb MS, Shu Y, Kuba H, Rasband MN, Wimmer VC, Bender KJ. Short- and long-term plasticity at the axon initial segment. Journal of Neuroscience. 2011;31(45):16049–16055. doi:10.1523/JNEUROSCI.4064-11.2011.

57. Yamada R, Kuba H. Structural and functional plasticity at the axon initial segment. Frontiers in Cellular Neuroscience. 2016;10: 00250. doi:10.3389/fncel.2016.00250.

58. Stimberg M, Brette R, Goodman DF. Brian 2, an intuitive and efficient neural simulator. eLife. 2019;8:e47314. doi:10.7554/eLife.47314.

59. Hirschmann F. rdp; 2014. Available from: `https://github.com/fhirschmann/rdp`.

60. Goethals S, Brette R. Theoretical relation between axon initial segment geometry and excitability. eLife. 2020;9:e53432. doi:10.7554/eLife.53432.

61. Kanemasa T, Gan L, Perney TM, Wang LY, Kaczmarek LK. Electrophysiological and pharmacological characterization of a mammalian Shaw channel expressed in NIH 3T3 fibroblasts. Journal of Neurophysiology. 1995;74(1):207–217. doi:10.1152/jn.1995.74.1.207.

62. Northcutt AJ, Fischer EK, Puhl JG, Mesce KA, Schulz DJ. An annotated CNS transcriptome of the medicinal leech, Hirudo verbana: De novo sequencing to characterize genes associated with nervous system activity. PLOS ONE. 2018;13(7):1–33. doi:10.1371/journal.pone.0201206.

63. Johansen J. Ion conductances in identified leech neurons. Comparative Biochemistry and Physiology Part A: Physiology. 1991;100(1):33–40. doi:https://doi.org/10.1016/0300-9629(91)90180-K.

64. Benda J, Herz AVM. A universal model for spike-frequency adaptation. Neural Computation. 2003;15(11):2523–2564. doi:10.1162/089976603322385063.

65. Dask Development Team. Dask: Library for dynamic task scheduling; 2016. Available from: `http://dask.pydata.org`.

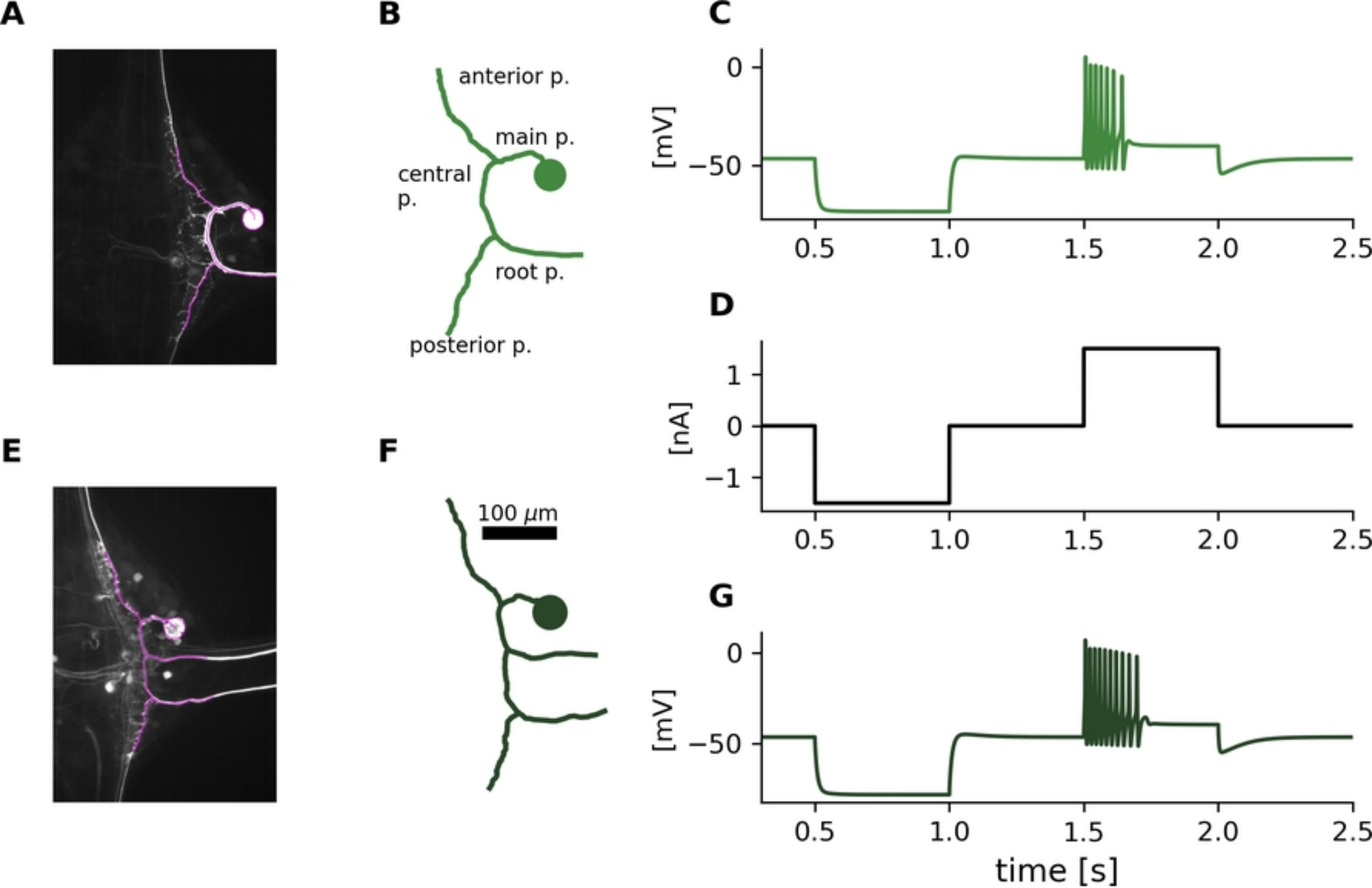
A
B
anterior p.
main p.
central p.
root p.
posterior p.
C
0
−50
[mV]
0.5
1.0
1.5
2.0
2.5
D
1
0
−1
[nA]
E
F
100 μm
G
time [s]

Figure 1

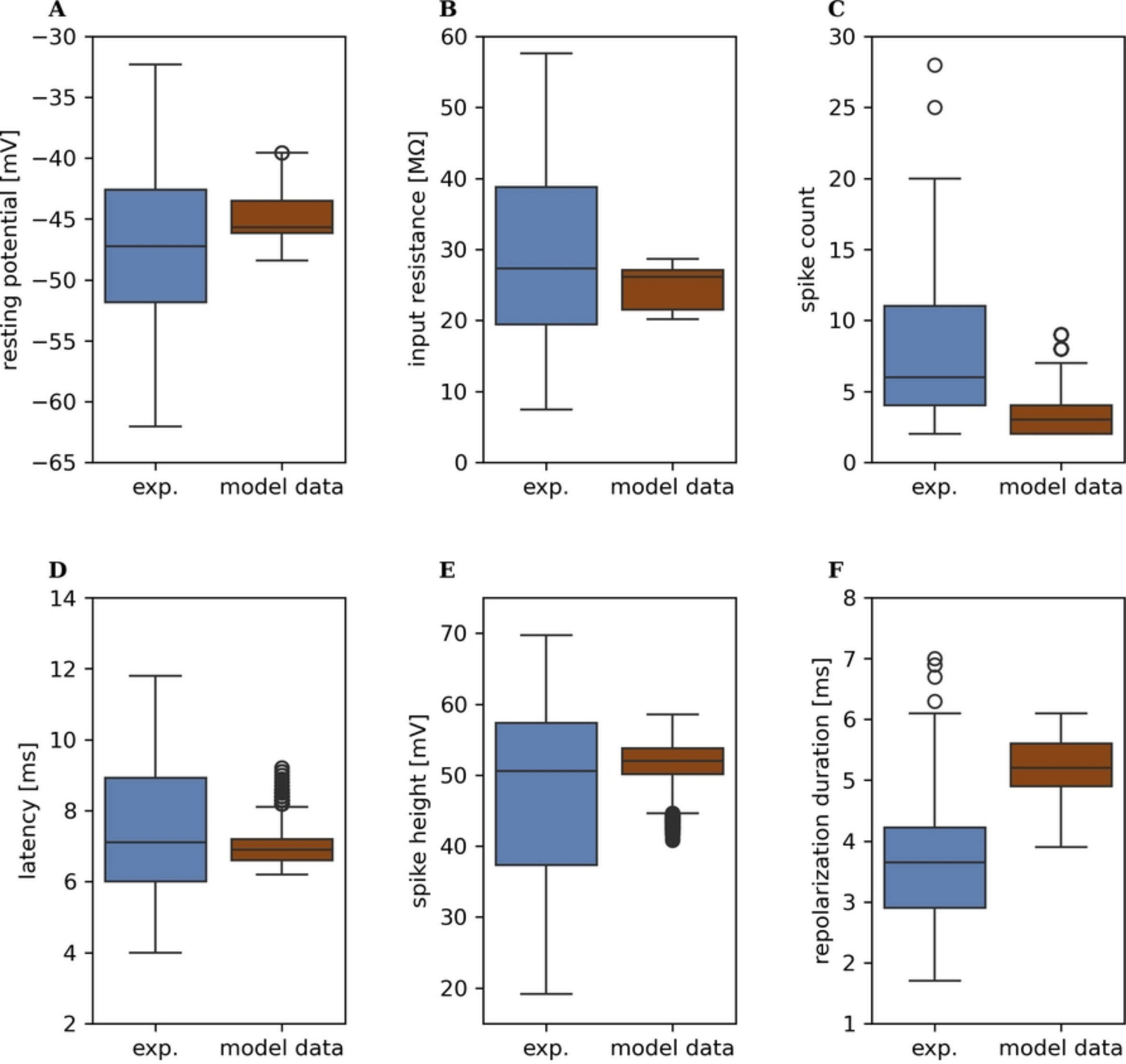
A
resting potential [mV]
−30
−35
−40
−45
−50
−55
−60
−65
exp.
model data
B
input resistance [MΩ]
60
50
40
30
20
10
0
exp.
model data
C
spike count
30
25
20
15
10
5
0
exp.
model data
D
latency [ms]
14
12
10
8
6
4
2
exp.
model data
E
spike height [mV]
70
60
50
40
30
20
exp.
model data
F
repolarization duration [ms]
8
7
6
5
4
3
2
1
exp.
model data

Figure 2

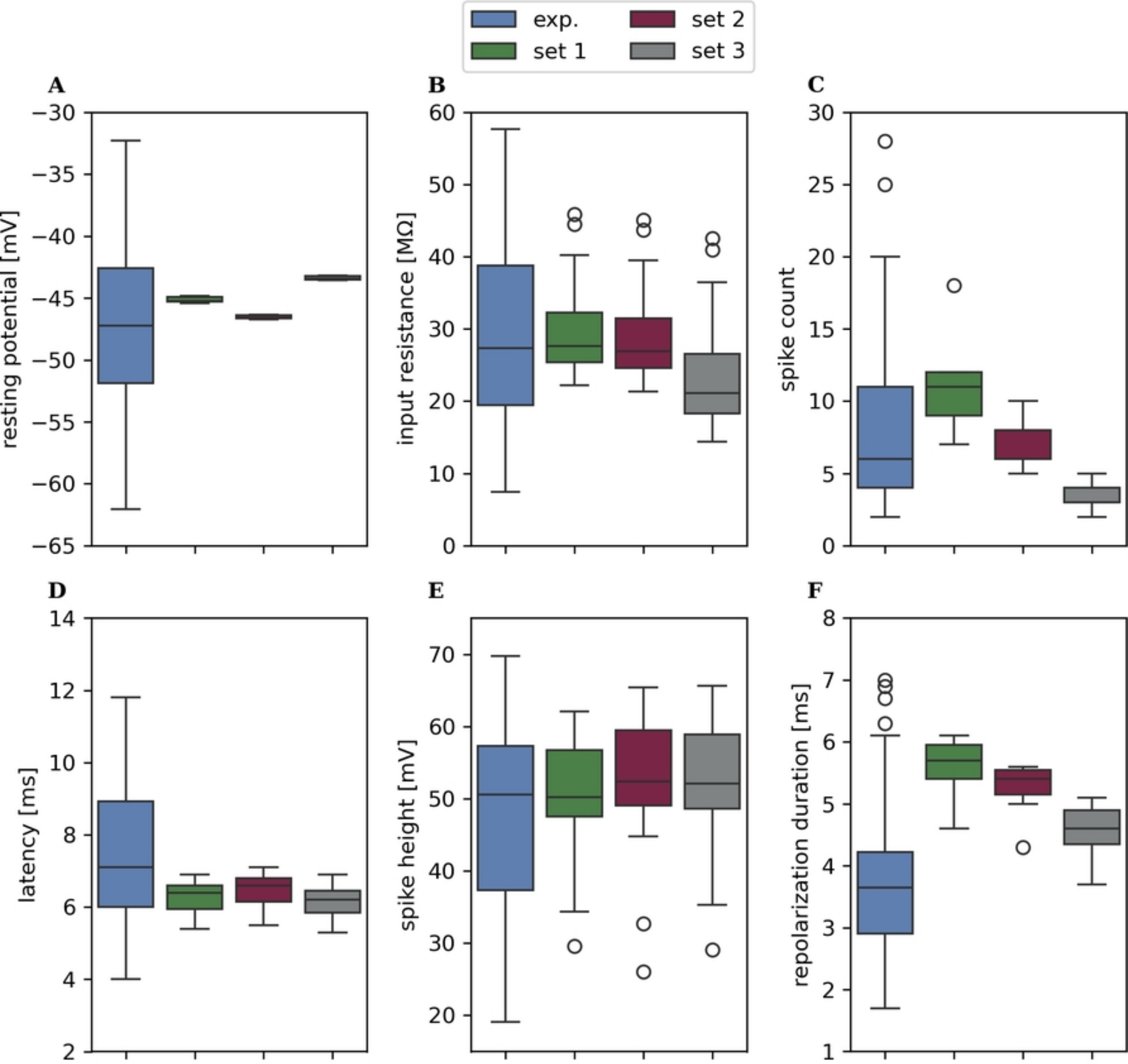
exp.
set 1
set 2
set 3
A
B
C
D
E
F
resting potential [mV]
input resistance [MΩ]
spike count
latency [ms]
spike height [mV]
repolarization duration [ms]

Figure 3

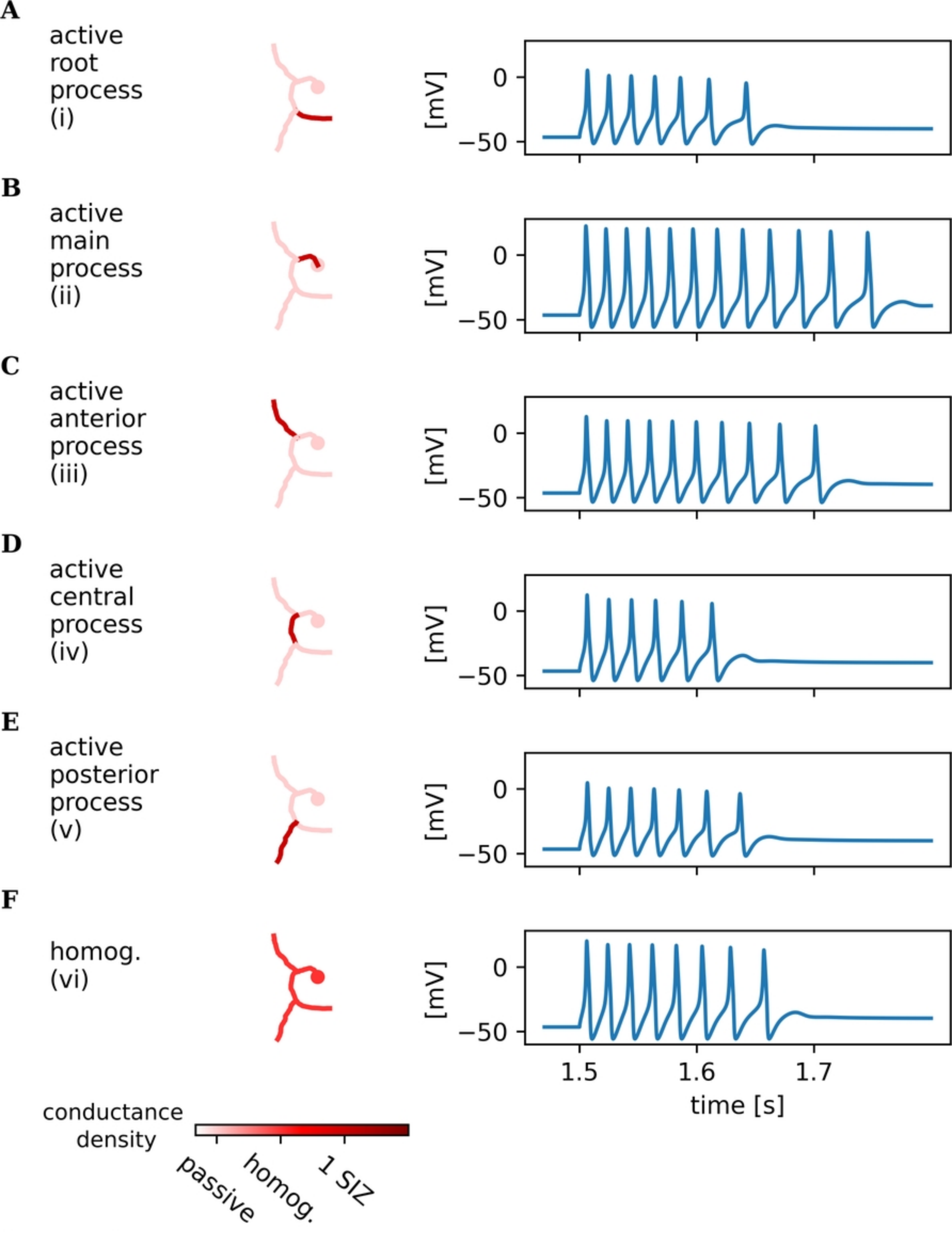
A
active
root
process
(i)
B
active
main
process
(ii)
C
active
anterior
process
(iii)
D
active
central
process
(iv)
E
active
posterior
process
(v)
F
homog.
(vi)
[mV]
0
−50
1.5
1.6
1.7
time [s]
conductance
density
passive
homog.
1 SIZ

Figure 4

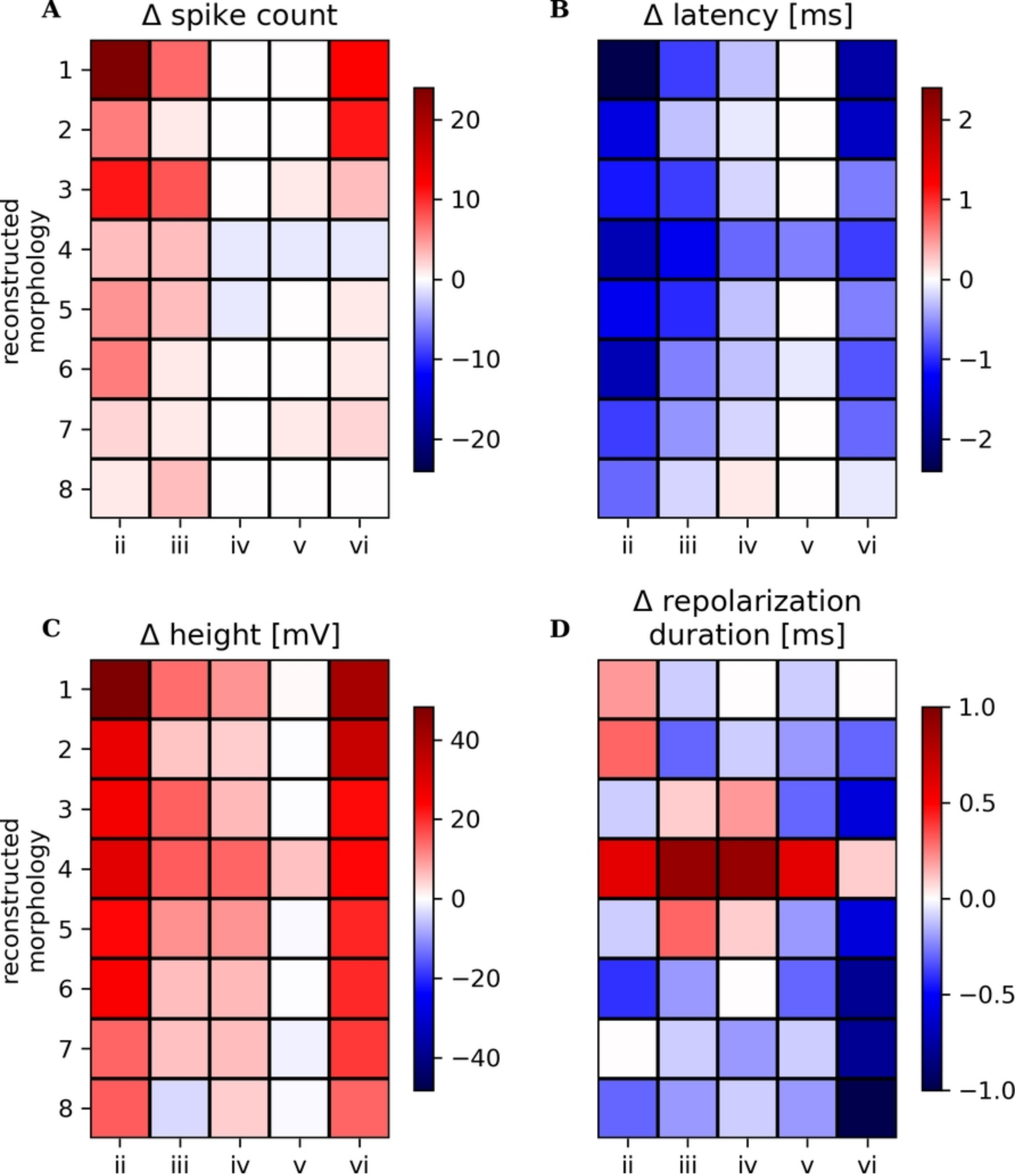
A
Δ spike count
B
Δ latency [ms]
C
Δ height [mV]
D
Δ repolarization duration [ms]
reconstructed morphology
1
2
3
4
5
6
7
8
ii
iii
iv
v
vi
20
10
0
−10
−20
2
1
0
−1
−2
40
20
0
−20
−40
1.0
0.5
0.0
−0.5
−1.0

Figure 5

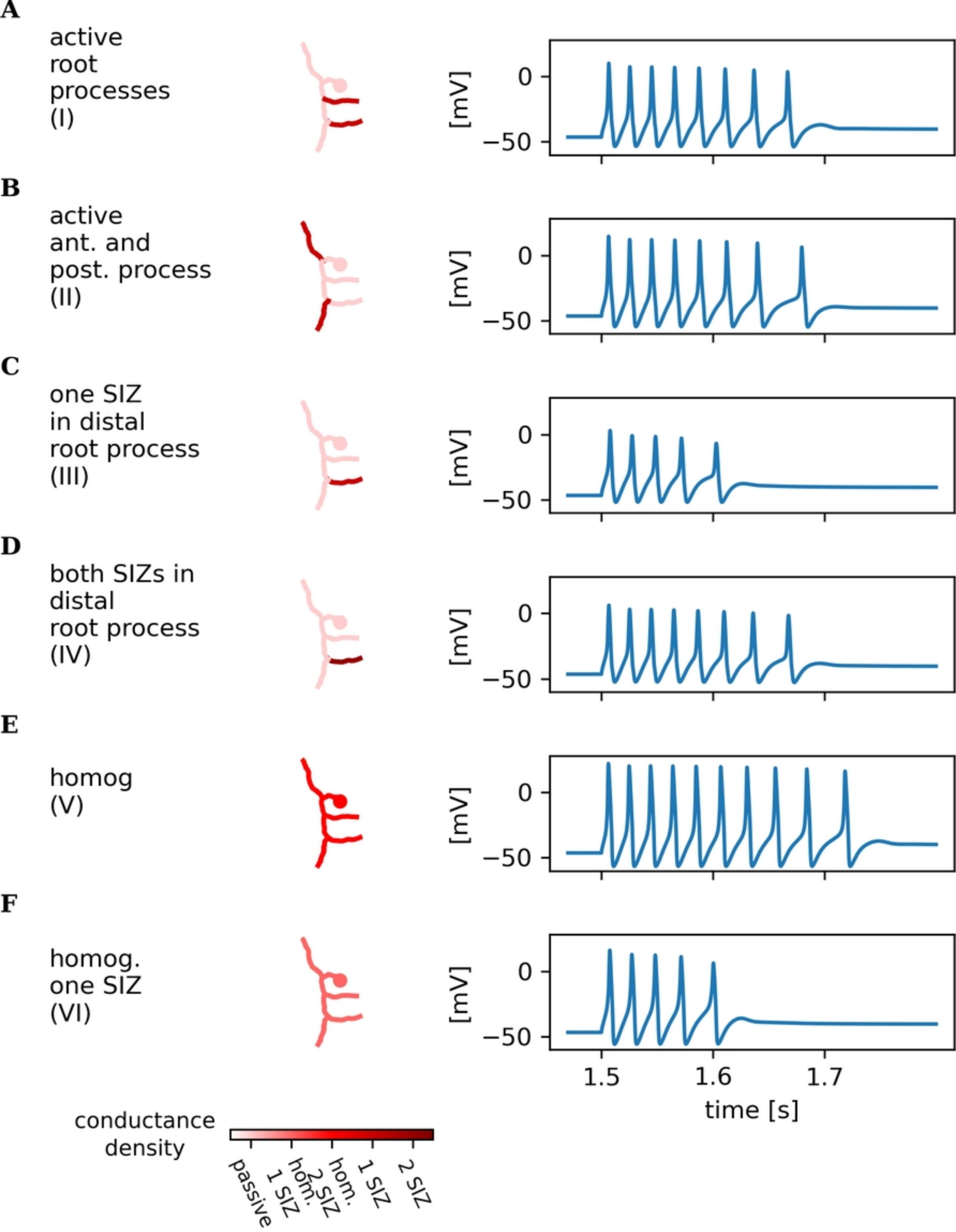
A
active
root
processes
(I)
B
active
ant. and
post. process
(II)
C
one SIZ
in distal
root process
(III)
D
both SIZs in
distal
root process
(IV)
E
homog
(V)
F
homog.
one SIZ
(VI)
[mV]
0
−50
1.5
1.6
1.7
time [s]
conductance
density
passive
1 SIZ
2 SIZ
hom.
hom.
1 SIZ
2 SIZ

Figure 6

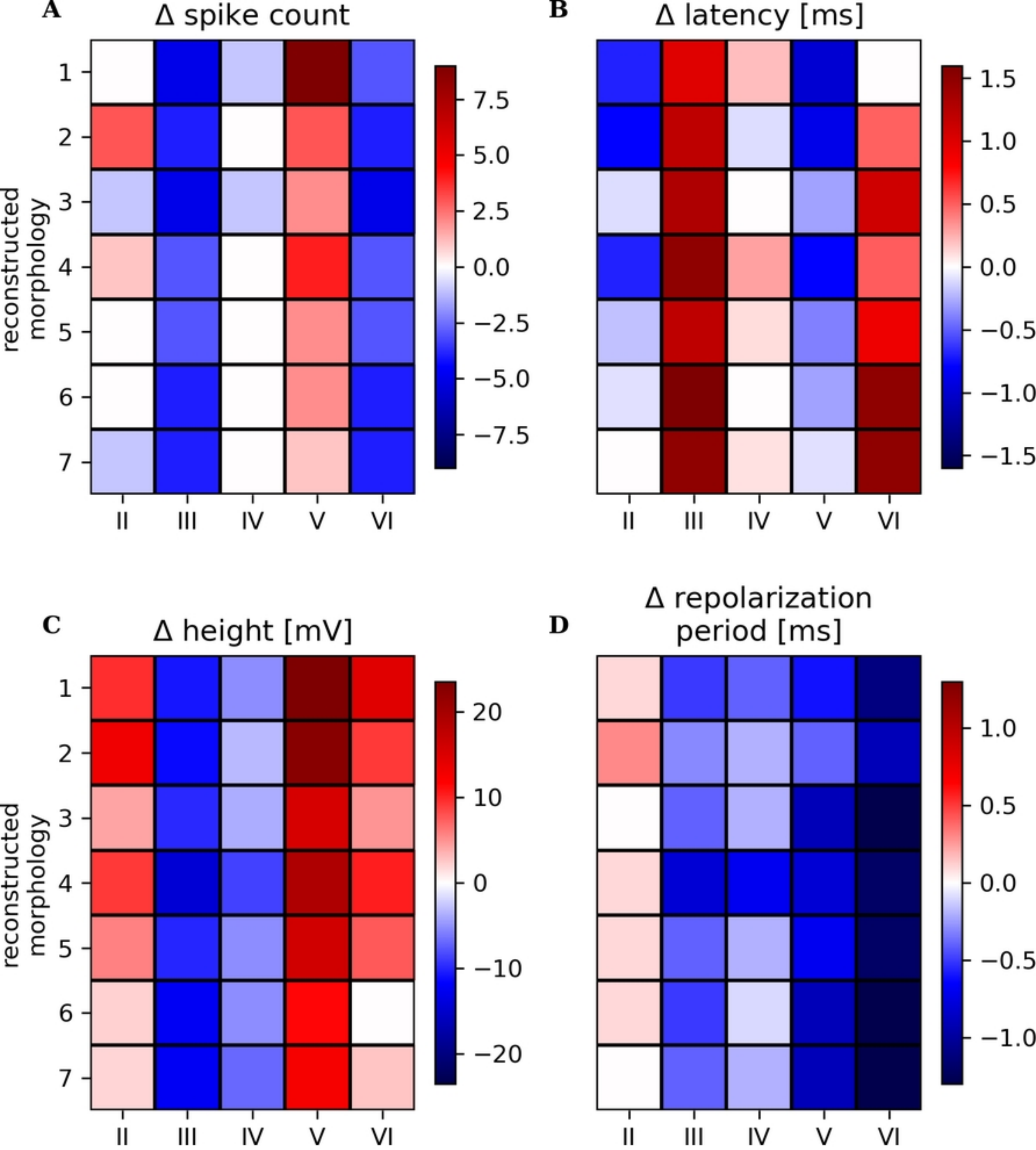
A
Δ spike count
B
Δ latency [ms]
C
Δ height [mV]
D
Δ repolarization period [ms]
reconstructed morphology
1
2
3
4
5
6
7
II
III
IV
V
VI
7.5
5.0
2.5
0.0
−2.5
−5.0
−7.5
1.5
1.0
0.5
0.0
−0.5
−1.0
−1.5
20
10
0
−10
−20
1.0
0.5
0.0
−0.5
−1.0

Figure 7

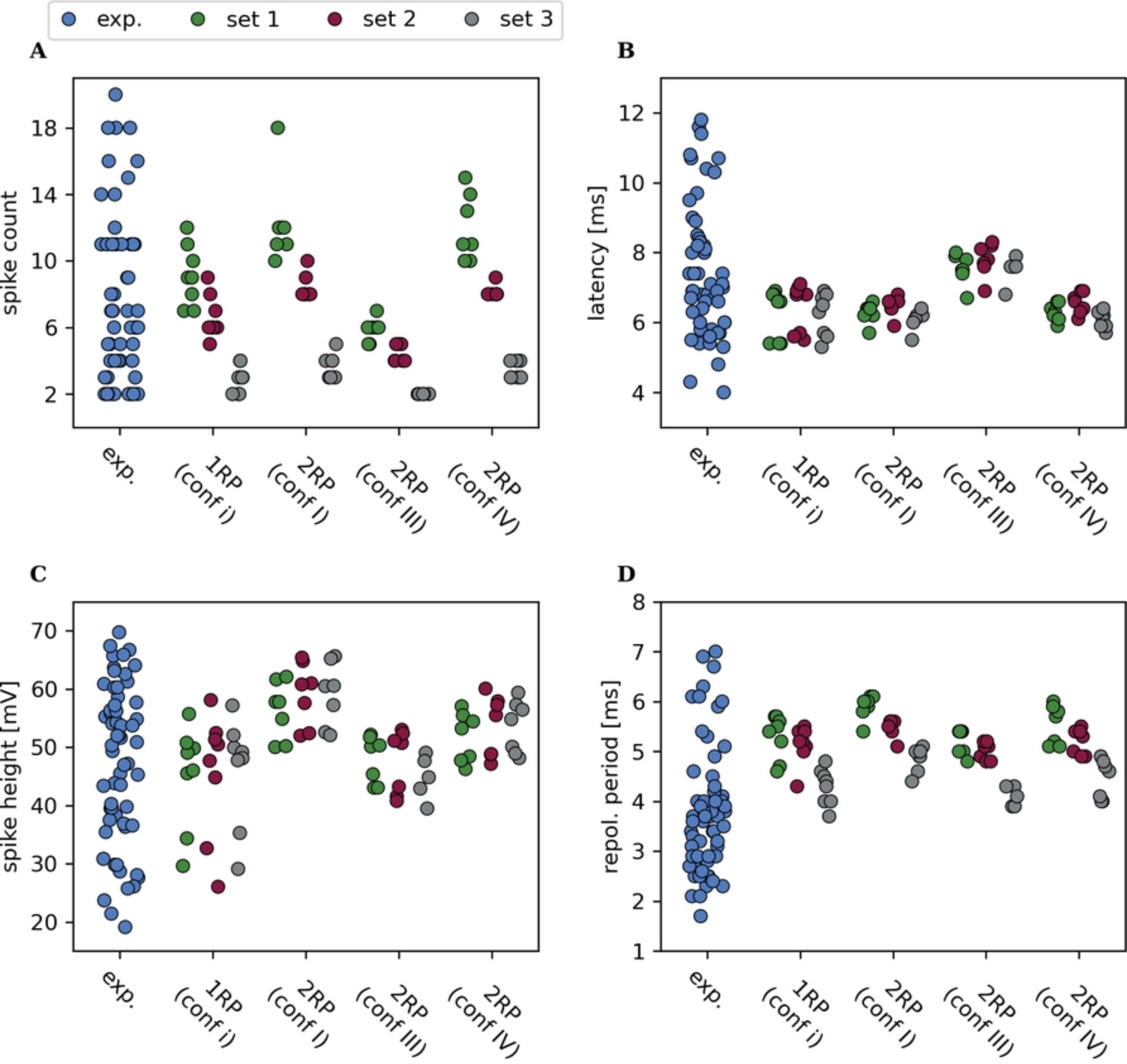
exp.
set 1
set 2
set 3
A
B
C
D
spike count
latency [ms]
spike height [mV]
repol. period [ms]
exp.
1RP (conf i)
2RP (conf I)
2RP (conf III)
2RP (conf IV)

Figure 8